WILDFIRE SMOKE ANALYSIS USING THE 760 NM OXYGEN ABSORPTION FEATURE

Daniel Schläpfer[1], Ian B. McCubbin[2], Bruce Kindel[3], Johannes W. Kaiser[1], and Eyal Ben-Dor[4]

1. University of Zurich, Zurich, Switzerland, dschlapf@geo.unizh.ch, jkaiser@geo.unizh.ch
2. Bay Area Environmental Research Institute, NASA Ames, USA, imccubbin@mail.arc.nasa.gov
3. CSES University of Colorado at Boulder, USA, kindel@cires.colorado.edu
4. Remote Sensing Research Center, Tel Aviv, Israel, bendor@post.tau.ac.il

ABSTRACT

In October 2003 the Santa Susanna Mountains, located to the northwest of Los Angeles, CA, sustained severe wild fires. The Airborne Visible and Infrared Imaging Spectrometer (AVIRIS) acquired four meter spatial resolution data over the burning area to assess the impact of the fires on the wildland to urban interface. Additional goals of the flights were testing the capabilities of airborne hyperspectral sensors as tools for fire monitoring, fire model validation, and the validation of space borne systems fire fuel products such as the Moderate Resolution Imaging Spectrometer (MODIS). The acquired imagery shows strong variations of smoke, including full a large plume of smoke from the burning areas to a height of 15 kilometers. As expected, the variability in smoke concentrations corresponded to a strong variability in aerosol concentrations. Thus, a pixel wise method of smoke detection, respectively for aerosol analysis, was required to address the significant variability in the data.

This paper evaluates the potential of the oxygen absorption band at 760 nm for the detection of smoke density in this rugged terrain. An analytical solution for the atmospheric path radiance term as observed by the AVIRIS system is first derived and presented. Alternatively, an iterative approach is given, where the spatial appearance of transmittance is optimized against the aerosol contents.

The results are validated against the surface reflectance, terrain shape, and the short wavelength smoke distribution patterns that show reasonable spatial match but non reasonable absolute path radiance values. A sensitivity analysis of the method is currently in process using a synthetic scene of the area under study. We show a promising potential of using the oxygen feature for aerosol mapping. Furthermore, the advantage and the problems of using spectrally highly resolved instruments (such as APEX) for aerosol retrieval in narrow absorption features on a pixel by pixel basis are outlined.

INTRODUCTION

The monitoring of smoke is directly related to methods monitoring aerosols remotely (1). Smoke monitoring is of high relevance for disaster monitoring applications and for air pollution analysis. The related parameter of interest is aerosol optical thickness (AOT), whereas particle size distribution and spherical albedo are further parameters of relevance. The optical properties of aerosols as well as the surface are highly variable in time and space, specifically if recent smoke is observed. As such, a pixel wise method for aerosol retrieval would be of high value. The goal of this presented ongoing work is to evaluate and find appropriate methods for aerosol and smoke analysis using spectrally and spatially high resolution instruments such as the upcoming Airborne Prism Experiment (APEX, (2)). The unique features of the instrument promise to potentially detect atmospheric constituents at high resolution. This will serve to increase atmospheric correction accuracies (3) as well as for atmospheric monitoring tasks (4).

Early studies on the retrieval of aerosol properties from satellite data over land were aimed at atmospheric correction. The 5S development (5) is an example of a simplified radiative transfer code being applied to the atmospheric correction problem. Often, dark object based methods had been used for that purpose in the past (6). These aerosol retrieval methods are commonly referred to as dark target approaches. They yield estimates of the AOT based on the increase in sensor level signal induced by aerosol backscattering and work on a per-image basis.

Newer developments had been extending to brighter objects by accounting for the strength of vegetation signatures in each pixel (7 and 8). In this methods, the surface reflectance was

separated from the spectral aerosol signatures for a specific range of objects. The retrieval of aerosol parameters has also been demonstrated with multi-temporal data from the Geostationary Orbit Environmental Satellite (GOES (1)). Multi-temporal analysis would be of interest for smoke analysis with regard to comparing a smoke free-scene of the same area to a later scene affected by smoke signatures. Karnieli et al., 2001 (9) have shown that it is possible to use the SWIR region in order to re-construct clear VIS region channels to calculate vegetation index over smoke areas.

Recently, a retrieval methodology was developed making use of near-UV spectral bands to retrieve aerosol parameters (10). Since the surface properties in the near-UV (0.38 and 0.4 mm) offer the advantage of low surface reflectance and weak bidirectional reflectance distribution function (BRDF) effects, variations of at-sensor radiance are mainly due to changing atmospheric influence. Thus, calculating the Rayleigh scattering with high accuracy will enable retrieval of the aerosol parameters, such as optical thickness and single-scattering albedo (11). These algorithms also enable to distinguish between non-absorbing particles and absorbing material. It bears the potential to be used with high accuracy hyperspectral instruments.

Investigated in this paper is the idea of using the effect of atmospheric scattering within gaseous absorption features. The inversion of a differential absorption technique would allow an estimatation of the total path radiance in each pixel individually (12). The total aerosol optical thickness could then be derived directly from the path radiance.

METHOD DESCRIPTION

Gaseous absorption in the atmosphere interacts with the atmospheric scattering: strong scattering processes lead to higher absorption within the absorption feature compared to lower scattering conditions. The relation between the relative depth of gaseous absorption features and aerosol scattering has been shown by various sources (13,14). A method for deriving aerosol concentration from the oxygen absorption feature was first given by Ben-Dor, 1994 (13), while the relation between aerosol concentration and atmospheric absorption was used in the APDA water vapor method for high accuracy trace gas retrieval (14).

The basic description of a relative absorption depth due to gaseous absorption was there given by:

$$T_{O_2} \approx R = \frac{L_m - L_{p,m}}{\sum_i w_i (L_{r,i} - L_{p,r,i})}, \text{ where} \qquad \text{(Eq. 1)}$$

L_m is the radiance measured in the oxygen 'measurement' band within the absorption feature, $L_{p,m}$ is the atmospheric path radiance in the same spectral band, $L_{r,i}$ is the at-sensor radiance in a non-absorbing reference bands i with its associated path radiance $L_{p,r,i}$, and w_i are the relative weights of the reference bands. The ratio number R is a good approximation for the oxygen transmittance for a direct path (T_{O_2}).

Note that the sharp shape of the oxygen feature enables a precise measurement of the absorption peak only if hyperspectral instruments with resolution better than 15 nm are used. One single measurement band in the center of the feature may be engaged for that purpose.

Now it is assumed, that the atmospheric path radiance within the oxygen absorption band is linearly related to the path radiance outside an absorption band such that you may write a linear relation:

$$L_{p,r,i} \approx q_i L_{p,m} . \qquad \text{(Eq. 2)}$$

The coefficient q_i of this linear relation may be derived from simulations and are constant for each combination between a reference band and the absorbing band. For theoretical reasons, no offset is included in the linear relation (if the path radiance is zero, it should be zero in all spectral bands). The validity of the assumption in Eq. 2 is shown with a MODTRAN simulation, where the path radiance dependency with spectral band and aerosol optical thickness is simulated over a zero albedo surface. The calculated deviations from the linear assumption are well below 1% at a maximum of 0.7%. The respective path radiance terms and the linear relationships are depicted in Figure 1. The figure also shows the inversere relationship between path radiance and aerosol

concentrations (i.e the path radiance is relatively large within an absorption feature at low aerosol concentration, whereas the relative path radiance is lower at higher concentrations).

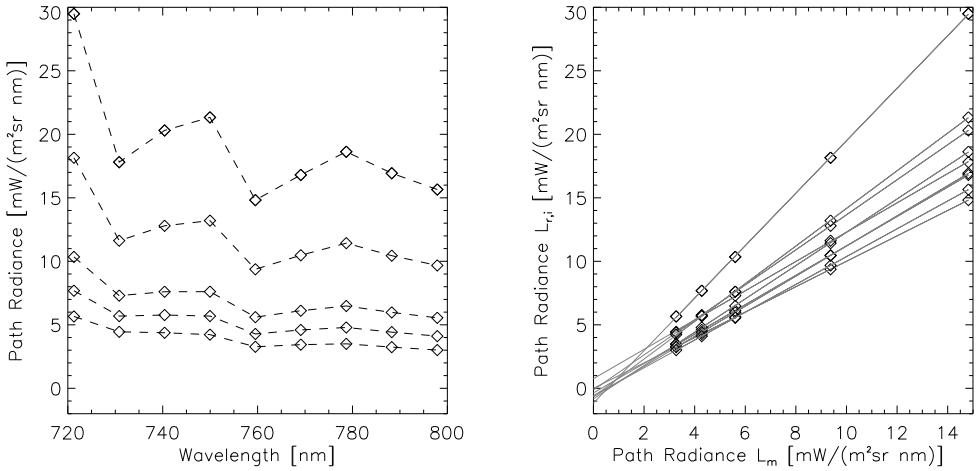

Figure 1 Path radiance term at albedo=0 in the range of the 760 nm oxygen absorption for the investigated AVIRIS (10 nm resolution) case.
Left: atmospheric path radiance at 0, 500, 1000, 1500 and 2000 m surface elevation.
Right: linear relation of the path radiance in the 8 bands outside absorption feature (as of the left figure) to path radiance within the feature at 760 nm.

Eq. 1 can now be reformulated to

$$T_{O_2} = \frac{L_m - L_{p,m}}{\sum_i w_i (L_{r,i} - q_i L_{p,m})} \qquad \text{and} \qquad T_{O_2} \sum_i w_i (L_{r,i} - q_i L_{p,m}) = L_m - L_{p,m}$$

which finally leads to an expression for the path radiance within the absorption band as:

$$L_{p,m} \approx \frac{L_m - T_{0_2} \sum_i w_i L_{r,i}}{1 - T_{0_2} \sum_i w_i q_i}. \qquad \text{(Eq. 3)}$$

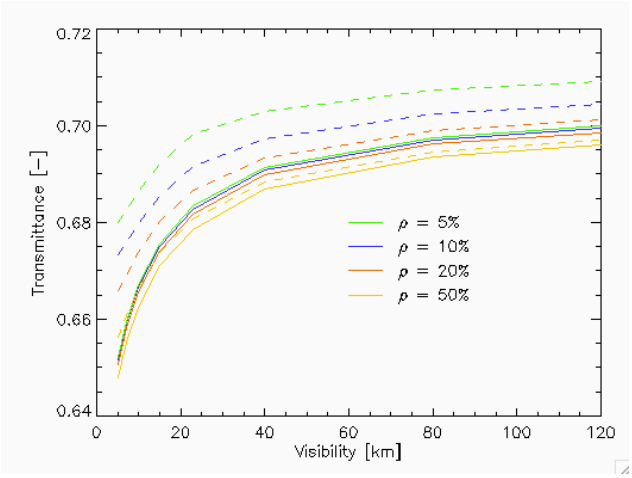

Figure 2 Variation of the apparent oxygen transmittance in relation to the horizontal atmospheric visibility at various surface reflectance values. The dashed curves are the apparent transmittances before correcting the path radiance effect while the solid lines are after atmospheric path radiance has been subtracted.

This equation shows the path radiance variations in relation to oxygen transmittance and to the measured at sensor radiance values.

The problem in the application of Equation 3 is the variations of oxygen transmittance due to changes in albedo and aerosol characteristics. The apparent transmittance is influenced by spherical albedo of the aerosol as well as by the surface reflectance function which both interact in multiple scattering processes. Thus, a refinement of this function needs to be found. The dependence on surface albedo is low as can be seen in Figure 2.

T_{0_2} itself thus mainly depends on the aerosol load, despite its dependence on the terrain altitude, h. Thus, a further parameterization can be introduced with:

$$T_{O_2,h} \approx T_{O_2,0,h} - a_h L_{p,m}, \qquad \text{(Eq. 4)}$$

which describes the relation of transmittance from the path radiance term on a surface altitude level *h*. The factor a_h is the height-dependent linear relation factor between direct oxygen transmittance and path radiance within the absorption band. MODTRAN simulations show that the linear relationship holds true within an accuracy of better than 1% for the altitude range under investigation (further refinement of the procedure could be done by using a non-linear relationship instead of Eq. 4). Using Equation 4, a further transformation of Equation 3 is required to obtain the path radiance term:

$$(T_{O_2,0,h} - a_h L_{p,m})\left[\sum_i w_i (L_{r,i} - q_i L_{p,m})\right] = L_m - L_{p,m}$$

$$\sum_i T_{O_2,0,h} w_i (L_{r,i} - q_i L_{p,m}) - \sum_i w_i a_h L_{p,m} (L_{r,i} - q_i L_{p,m}) = L_m - L_{p,m},$$

solving for the path radiance term yields in the case of two reference bands (i=1,2):

$$\begin{aligned} & L_m - T_{O_2,0,h}\left(w_1 (L_{r,1} - q_1 L_{p,m}) + w_2 (L_{r,2} - q_2 L_{p,m})\right) \\ &= L_{p,m} - w_1 a_h L_{p,m} (L_{r,1} - q_1 L_{p,m}) - w_2 a_h L_{p,m} (L_{r,2} - q_2 L_{p,m}) \\ &= L_{p,m} \cdot \left(1 - w_1 a_h L_{r,1} - w_2 a_h L_{r,2}\right) + {L_{p,m}}^2 \left(w_1 a_h q_1 + w_2 a_h q_2\right) \end{aligned}$$

One last reformulation gives a quadratic equation for the path radiance term $L_{p,m}$:

$$\begin{aligned} & L_m - T_{O_2,0,h}\left(w_1 L_{r,1} + w_2 L_{r,2}\right) \\ &= L_{p,m} \cdot \left(1 - a_h \left(w_1 L_{r,1} + w_2 L_{r,2}\right) - T_{O_2,0,h}\left(w_1 q_1 + w_2 q_2\right)\right) \\ & \quad + {L_{p,m}}^2 \left(w_1 a_h q_1 + w_2 a_h q_2\right) \end{aligned} \qquad \text{(Eq. 5)}$$

This is a standard quadratic equation with two solutions. From the two solutions, the one with the lower relative variation of path radiance is taken (i.e., the one which does not exhibit the surface reflectance structure). This analytical approach is elegant – but it does not lead to plausible test results (see next section).

A second procedure has therefore been applied in contrast to the one as of Equation 5. Retrieving the oxygen transmittance directly from the image is not feasible as Equation 1 holds two unknowns, and no other equation is available. Thus solving the problem through image statistics might be the solution. The oxygen transmittance image needs to be a spatially smooth function. Now, take equations 1 and 2 again and proceed differently: a scaling factor a is put into the equation for scaling the originally assumed path radiance terms, such that

$L_{p,i} = L_{p,i,\min} + k(L_{p,i,\max} - L_{p,i,\min})$, and

$$T_{oxy} = \frac{L_m - L_{p,m,\min} - k(L_{p,m,\max} - L_{p,m,\min})}{\sum_i w_i (L_{r,i} - L_{p,r,i,\min} - k(L_{p,r,i,\max} - L_{p,r,i,\min}))} \quad \text{(Eq. 6)}$$

The scaling factor k is iteratively tuned until a smooth appearance of the oxygen transmittance image is detected on the basis of its relative standard deviation. The path radiance can then be derived as the product between original and final value.

SIMULATION EXAMPLE

An example to demonstrate the above is given by a simulated AVIRIS scene. The simulated image holds varying visibility values ranging from 0 to 100 km (1km increment) in the across track direction and surface albedo values ranging from pure vegetation to pure soil (1% increment) in the along track direction. Also this image is characterized by a water vapour content of 1cm along the entire scene and altitude value of sea level. Figure 3 shows the radiance spectra obtained at a selected target (50% vegetation + 50% soil) in a path radiance's cross section. As seen, the path radiance in this target decreases the oxygen feature value as going from 100 km to 0 visibility.

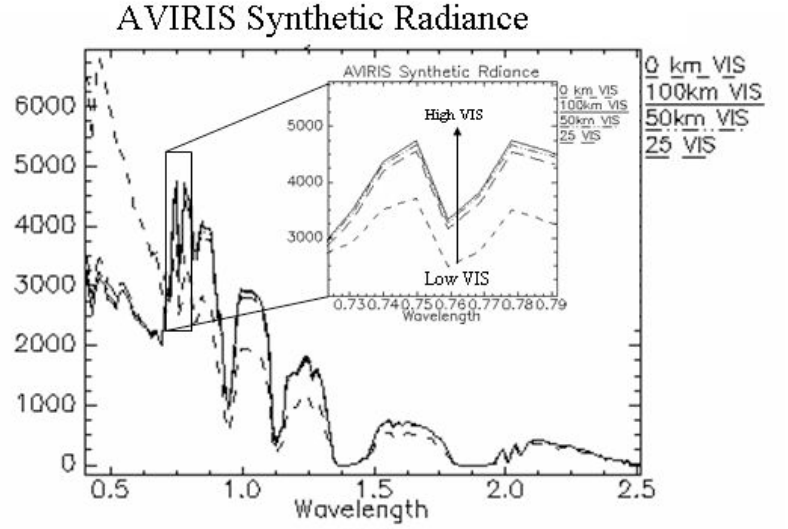

Figure 3: The radiance of 50% vegetation + 50% soil over varying path radiance values as expressed in visibilities values

Plotting $L_m / L_{p,m}$ (in three selected mixed targets positions) against the visibility is depicted in Figure 4, where L_m stands for the radiance measured in the oxygen 'measurement' band within the absorption feature and $L_{p,m}$ stands for the radiance reading at this band if no (oxygen) absorption occurs.

We get, for each of the mixed target selected, a different function F(VIS) that can be further used to calculate the k factor to correct for the path radiance in a given pixel. This calculation brings the "contaminated" treated pixel to hold a "new" target with path radiance equivalent to 100km visibility (in which we assume that $L_{p,m} = 0$). The calculation is made as follows:

$$\left(L_m / L_{p,m}\right)_{100\,km} - \left(L_m / L_{p,m}\right)_{image} = k$$

The 100km-value of this equation can be generated from the F(VIS) function and then can be further used as a constant value (N) to form the following new equation:

$$N - \left(L_m / L_{p,m}\right)_{image} = k$$

This calculation can then be applied on a pixel by pixel basis to obtain a path clear image. Since the path radiance is a function of the k parameter, the path radiance image can be generated by subtracting the original and clear AVIRIS image.

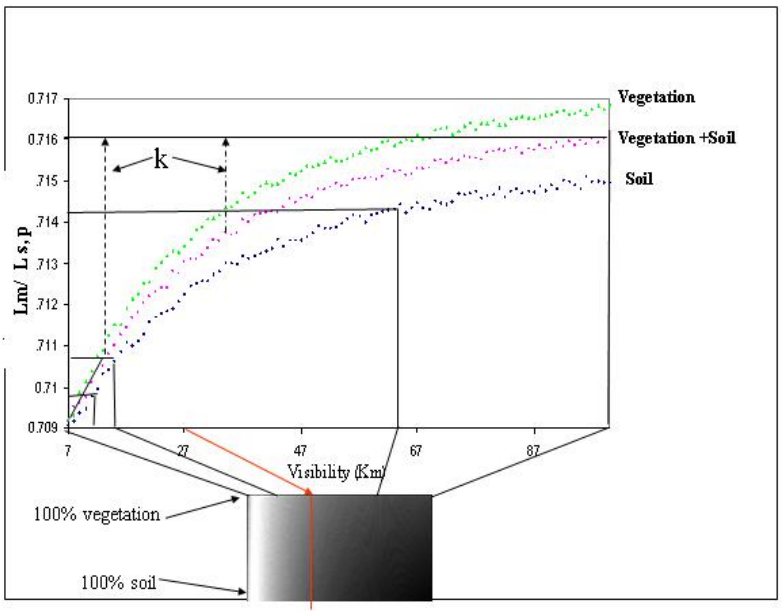

Figure 4 The relationship between Lm/Lp,m and the visibility in three different surface targets: 100% vegetation, 50% vegetation+50% soil, 199% soil in a simulated AVIRIS scene.

Figure 5 shows the simulated image as generated using the oxygen feature in the original (uncorrected) image(a) holding aerosols, the $L_m / L_{p,m}$ image from which k was generated (b) that is correlated with the path radiance, and the corrected image (c) in the oxygen feature that shows a clear constant soil - vegetation image at any path radiance values (correctd). This significantly shows that in the simulated hyperspectral environment, the oxygen feature can be used as an internal marker to correct for the path radiance.

The main disadvantageous of this method is that a pre-classification of the image is required. However this classification needs relatively less accuracy than a fine tuning atmospheric correction. In this regard a rough estimation of the targets in question can be done (eg. using NDVI classifier) in order to select an optimal look-up-table function for correcting the pixel's path radiance.

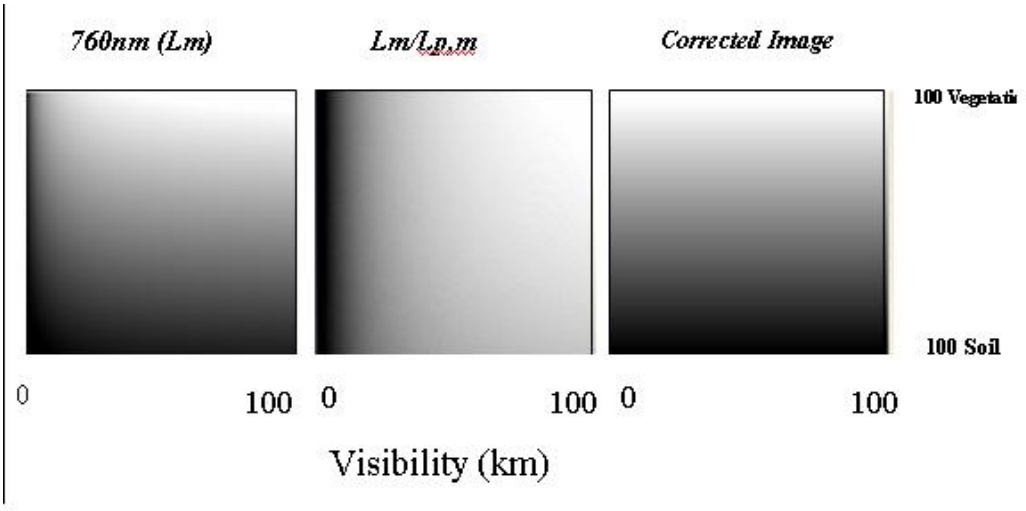

Figure 5 The simulated AVIRIS image at the absorbance oxygen feature in the "aerosols contaminated" image (a), the Lm/Lp,m (path radiance) image (b) and the corrected soil-vegetation image (c).

DATA BASIS

The method is tested on AVIRIS data taken on October, 27th 2003, 22:05 GMT, at an average geographical position of 34.3 deg north and 118.7 degrees west. This late-year situation leads to a solar zenith angle at 58.6 degrees. The data was acquired at 5600 m. above sea level, while the surface altitude varies between 280 and 880 meters. The area is located adjacent to the San Fernando Valley urban region along the Santa Susanna mountain range in Southern California. The data has been orthorectified to an accuracy of 1-2 pixels using the PARGE orthorectification method (15), a 10m-resolution USGS DEM and a number of 8 ground control points. A scene overview in both the RGB and SWIR domain is given in Figure 6. The radiance hardly passes the smoke at low wavelengths while in the SWIR, the smoke is optically transparent.

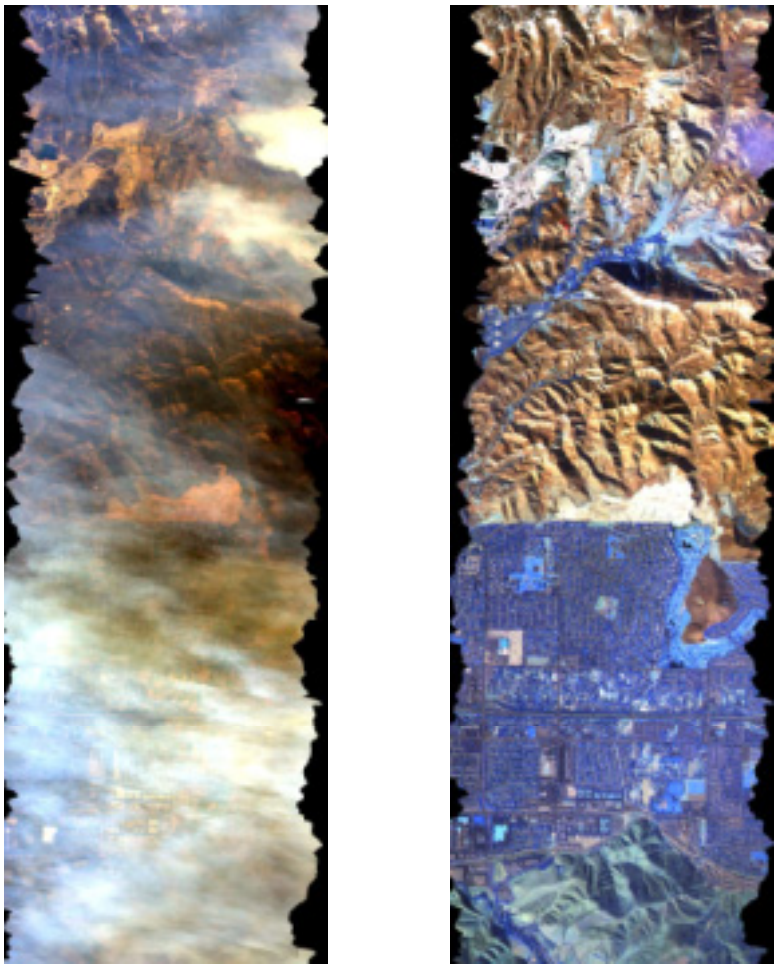

Figure 6 Orthorectified test AVIRIS 2003 scene 'Simi Valley' - left: RGB display (bands 34/20/8) showing the heavy smoke, right: NIR/SWIR composite (bands 200/140/75).

AVIRIS data was first acquired at the same site in 1999 at 20 m spatial resolution for species identification of the local Chaparral ecosystem, which is the dominant vegetation community in the Southern California Mountains. The Chaparral vegetation communities are dependent on wildfires for re-growth and fire fuel suppression. The fires typically occur on an approximately 50 year time cycle. Over the last century fire suppression has allowed for production of an abundance of fire fuels, and thus have become a high risks for the urban areas that border the ecosystems. The 1999 data allowed for a pre-fire baseline to compare with the 2003 data. Both datasets are first orthorectified to a digital elevation model. The Orthorectification allows for a direct comparison of the two datasets as well as the calculation of the normal distribution of oxygen in the image based on the surface pressure (as oxygen is uniformly distributed).

RESULTS

The two proposed methods have been applied to the AVIRIS data. When taking Equation 5, two solutions are returned from the quadratic expression. The first solution show an average of 2.75± 0.41 mW/(cm^2 sr nm), which is higher than the average radiance in the measurement band at 2.5± 0.45 mW/(cm^2 sr nm). Furthermore it shows a strong dependency on the surface reflectance and as such is rejected as a reasonable solution. The second solution of Equation 5 for the atmospheric path radiance term is spatially smooth and visually correlates well with the observed smoke signatures at shorter wavelengths (see Figure 7). However, the correlation is negative and its average value is at –0.21±0.002 mW/(cm^2 sr nm). The absolute value of this result would be a very plausible path radiance term (as shown in Figure 7). Currently, we understand this as path-radiance related atmospheric feature which needs further investigation. We assume that an average shortening of the path due to single scattering at the smoke plumes leads to a higher oxygen transmittance and thus to a lower path radiance signal over clouds.

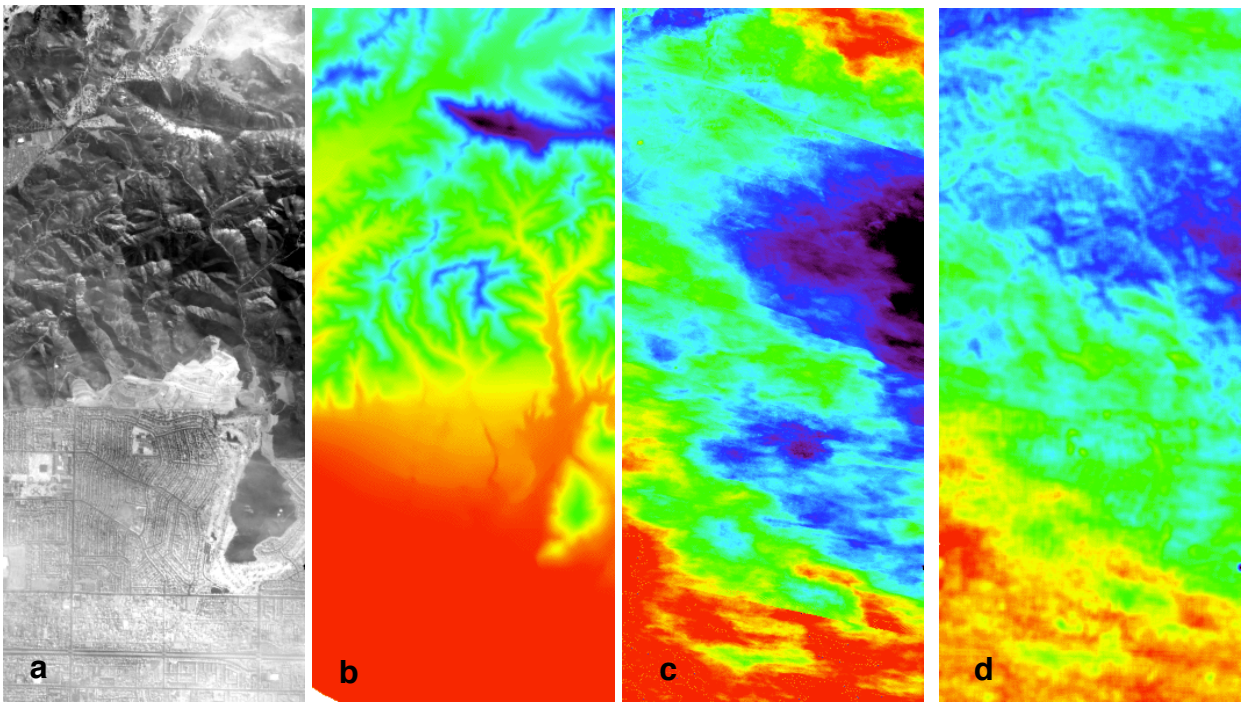

Figure 7 Retrieval of aerosol scattering influence on the oxygen transmittance following equation 5. From left to right: a) spectral radiance at 759 nm, b) digital elevation model (red=low), c) radiance at 404 nm (red=high radiance), d) (apparent) atmospheric path radiance signature (second solution of Eq. 5, red=low path radiance).

When using the second approach following Equation 6, the algorithm will not converge to a solution as long as the path radiance is varied within and outside the absorption feature. As soon as only the path radiance within the feature is varied, Equation 6 will converge to a physical solution as shown in Figure 8. The path radiance as derived through this method is related to the smoke as seen in Figure 7, left and shows no dependency on the surface reflectance characteristics. The quantitative values for the transmittance are 0.73 ± 0.00005 while the path radiance is varying at 0.12 ± 0.0002 W/(cm^2 sr nm). However, its accuracy needs to be assessed and certain discrepancies between the 404 nm image and the signature derived from the oxygen are waiting to be explained.

CONCLUSIONS

With the first analysis presented in this paper, we were able to provide a parameterization of the atmospheric path radiance term directly from a standard differential absorption in the 760 nm oxygen band. The presented method allows a solution for the path radiance term on a pixel basis. The resulting images for a test scene with heavy smoke show a spatially smooth signature, which is strongly correlated to the smoke distribution as shown at short wavelengths.

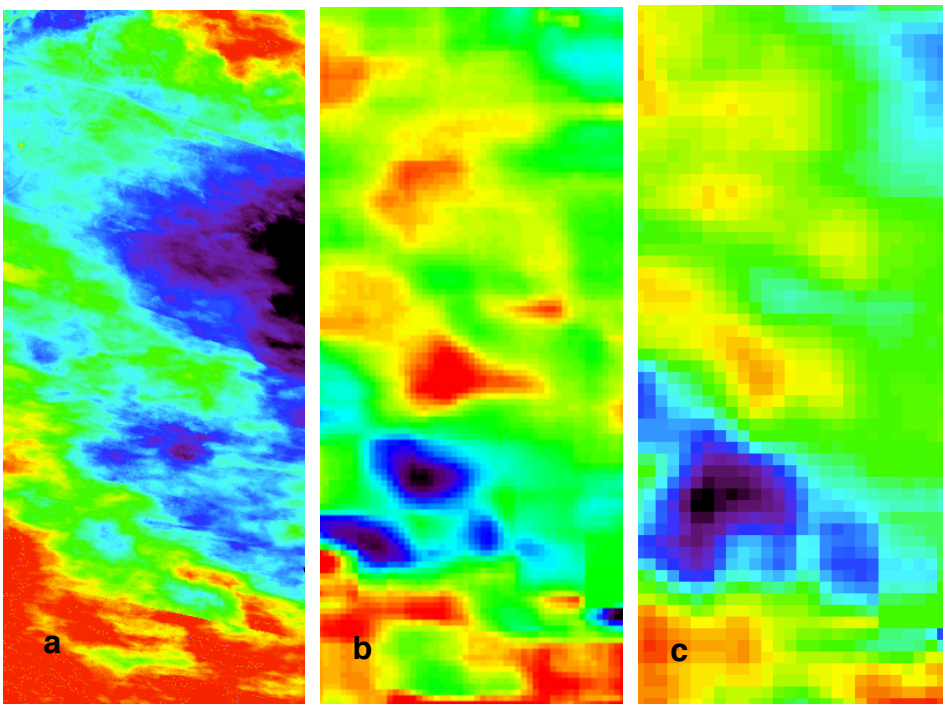

Figure 8 Atmospheric path radiance and transmittance value from iterative optimization procedure, scaling the path radiance in the measurement band only. From left to right: a) signature at 404 nm, b) iterative path radiance on 10 pixels resolution, and c) iterative path radiance at 20 pixels resolution. High values are depicted in red.

However, the range and sign of the calculated values are not within physical limits. The reason for this discrepancy might be that the underlying atmospheric look-up-table is not well suited as it assumes a logarithmic decay of aerosols with altitude, whereas the smoke has a totally different vertical distribution.

Using a spatially adaptive absorption technique, the range of the calculated path radiance term is closer to the expected values. Now, the spatial distribution is not as expected and requires quite some reasoning to be explained properly.

The obvious failure of the methods on real data may be due to various reasons which need further investigation:

- The used LUT for atmospheric situation was of generic nature. An explicit LUT for smoke situations coupled with reflectance properties that characterize the area in question may lead to more realistic results.
- The linear assumptions for the relation of the path radiance term to the oxygen transmittance may not be true for high aerosol loads.
- The representation of the LUT uses standard vertical profiles. Smoke has a vertical distribution which is slightly different and as such may not be easily be treated with the analytical equations we used so far.

Future work will thus focus on improving the LUT used for inversion. For a pixel wise classification, also methods using the 380-420 nm region of the spectrum will be taken into account towards the goal of a true pixel-wise mapping of aerosol signatures. But also the mixing approach as shown in the simulations is a promising way towards a robust hyperspectral aerosol retrieval algorithm using the oxygen-A absorption band.

ACKNOWLEDGEMENTS

Rolf Richter from DLR Munich is acknowledged for providing help using the ATCOR look-up-tables for this task. The AVIRIS team at JPL is thanked for providing the AVIRIS scenes including the ancillary data.

REFERENCES

1 Zhang J.L., Christopher S.A. and Holben B.N., 2001: Intercomparison of smoke aerosol optical thickness derived from GOES 8 imager and ground-based Sun photometers. Journal of Geophysical Research-Atmospheres, 106(D7): 7387-7397.

2 Nieke J., Itten K.I., Kaiser J.W., Schläpfer D., Brazile J., Debruyn W., Meuleman K., Kempeneers P.B., Neukom A., Feusi H., Adolph P., Moser R., Schilliger T., Quickelberghe M.V., Alder J., Mollet D., Vos L.D., Kohler P., Meng M., Piesbergen J., Strobl P., Schaepman M.E., Gavira J., Ulbrich G.J. and Meynart R., 2004: APEX: Current Status of the Airborne Dispersive Pushbroom Imaging Spectrometer. W. L. Barnes and J. J. Butler (Editors), Earth Observing Systems IX. Proc. SPIE, Vol. 5542, Maspalomas (Spain), pp. 109-116.

3 Richter R. and Schläpfer D., 2002: Geo-atmospheric processing of airborne imaging spectrometry data. Part 2: Atmospheric/Topographic Correction. International Journal of Remote Sensing, 23(13): 2631-2649.

4 Kaiser J.W., J. Nieke, D. Schläpfer, J. Brazile, & K.I. Itten, 2005: The atmospheric sensitivity of the airborne imaging spectrometer APEX, in: H. Fischer and B.J. Sohn (Eds.): IRS 2004: Current Problems in Atmospheric Radiation, A. Depaak Publishing, Hampton, Virginia, USA, submitted.

5 Tanré D., Herman M. & P.Y. Deschamps, 1983: Influence of the Atmosphere on Space Measurements of Directional Properties. Applied Optics, 22(5): 733-741.

6 Kaufman Y.J. & C. Sendra, 1988: Algorithm for Automatic Atmospheric Corrections to Visible and near-Ir Satellite Imagery. International Journal of Remote Sensing, 9(8): 1357-1381.

7 Hoyningen-Huene v. W., Freitag M. & J.P. Burrows, 2003: Retrieval of spectral aerosol optical thickness over land surfaces from top-of-atmosphere radiance, J. Geophys. Res., 108.

8 Bojinski S., Schläpfer D., Schaepman M., Keller J. and Itten K.I., 2004: Aerosol mapping over land with imaging spectroscopy using spectral autocorrelation. International Journal of Remote Sensing, 25(22): 5025-5047.

9 Karnieli A. Kaufman J. Y. And R.A.Wald 2001 AFRI – Aerosol free vegetation index. Remote Sensing of Environment 77:10-21.

10 Torres O., P.K. Bhartia, J.R. Herman, Z. Ahmad & J. Gleason, 1998: Deviation of aerosol properties from satellite measurements of backscattered ultraviolet radiation: Theoretical basis, J. Geophys. Res., 103.

11 Höller R., A. Higurashi, & T. Nakashima, 2004: The GLI 380-nm channel application for satellite remote sensing of tropospheric aerosol, EUMETSAT Meteorological Satellite Conference.

12 Schläpfer D., 1998: Differential Absorption Methodology for Imaging Spectroscopy of Atmospheric Water Vapor, Remote Sensing Series, Vol 31, RSL, Zürich, pp. 131.

13 Ben-Dor E., Goetz A.F.G. and Shapiro A.T., 1994: Estimation of Cirrus cloud and aerosol scatterin in hyperspectral image data, Proceedings of the International Symposion on Spectral Sensing Research. ISSSR, San Diego, CA, USA, Vol. II, pp. 582-590.

14 Schläpfer D., Borel C.C., Keller J. and Itten K.I., 1998: Atmospheric Pre-Corrected Differential Absorption Techniques to Retrieve Columnar Water Vapor. Remote Sens. Environ., 65(3): 353-366.

15 Schläpfer D. and Richter R., 2002: Geo-atmospheric processing of airborne imaging spectrometry data. Part 1: Parametric Ortho-Rectification Process. International Journal of Remote Sensing, 23(13): 2609-2630.